

IMPROVING THE IMPACT RESISTANCE OF MASONRY PARAPETS

*G. Beattie¹, T.C.K. Molyneaux², M.Gilbert³, B.Hobbs⁴,
S.Burnett⁵, P. Newton⁶, D.A.Gration⁷*

1 - Postgraduate Student, University of Liverpool, UK. Email:greg99@liverpool.ac.uk.

2 - Lecturer, University of Liverpool, UK. Email:ec116@liverpool.ac.uk.

3 - Lecturer, University of Sheffield, UK. Email: m.gilbert@sheffield.ac.uk.

4 - Postgraduate Student, University of Sheffield, UK. Email:cip99sjb@sheffield.ac.uk.

5 - Professor of Construction, University of Teesside, UK. Email b.hobbs@tees.ac.uk.

6 - Research Associate, University of Teesside, UK. Email:p.newton@tees.ac.uk

7- Associate, Arup Advanced Technology Group, UK.email:david.gration@arup.com.

1.0 Abstract

There are over 60000 masonry bridge parapets in the UK. Whereas steel and concrete parapets are well covered by design standards masonry parapets are not. Initially LS-DYNA was used to model vehicle impacts on various forms of masonry parapet. The results were encouraging, with good qualitative agreement between tests and analysis. The same finite element modelling strategy was subsequently used to help develop a guide for assessment (County Surveyors' Society Guidance Note, 1995) and a new British Standard (BS 6779 pt 4, 1999).

The findings of the initial study demonstrated that unreinforced masonry could perform reasonably well in preventing vehicle penetration and controlling the rebound of impacting vehicles. However the work highlighted two areas that required additional study: (i) in critical situations requiring improved impact resistance, advice on alternative strengthening methods or new build options was needed; (ii) the discrete analysis approach adopted, using LS-DYNA tied interface type 9, required use of unrealistic failure parameters in order to prevent a premature (brittle) failure.

The current project is addressing these two issues by the use of both physical tests and finite element analysis. The test work involves a range of small and medium scale tests that provide data for the numerical work. These tests address the issue of dynamic enhancement of the shear and tensile strength of masonry. In addition, the effects of fracture energy and dilatancy under high strain rates are being considered. Test methods have also been developed to evaluate the interaction between the masonry and reinforcement under varying strain rates. Full-scale tests are also being used to both provide analytical data in the early stages of the project and to validate the use of LS-DYNA as a predictive tool in the latter stages of the project. The full-scale test walls range from approximately 9m to 20m in length.

In the numerical models the existing LS-DYNA interfaces are being modified to incorporate the effects of fracture energy and dilatancy. Early results are promising, allowing realistic material properties to be used and seeming to explain the apparent high strain rate sensitivity of the measured data. Strategies for modelling reinforcement in a masonry wall are also being developed. Related work where LS-DYNA is being used to model masonry arch bridges is also summarised within this paper.

KEYWORDS: masonry, reinforced masonry, impact, parapets, fracture energy, dilatancy, masonry arch.

2.0 Background

Work by Molyneaux et al (1995) using LS-DYNA represented joints using nodes tied to discrete surfaces (LS-DYNA type 9 interface). In this approach, the nodes remain tied whilst failure criterion (1) is satisfied, after which the surfaces are free to separate or slide with friction.

$$\left[\frac{tension}{tension_{limit}} \right]^2 + \left[\frac{shear}{shear_{limit}} \right]^2 \leq 1 \quad (1)$$

Using the type 9 interface, the shear limit is assumed not to be affected by the presence of normal compression. The approach was used reasonably successfully to model brickwork and stone walls undergoing large deformations following vehicle impacts. However, to achieve good correlation between full-scale test data and the numerical results, enhanced (above normal quasi-static) values of the limiting stresses indicated in Equation 1 had to be used. The use of the higher values appeared justified as Molyneaux (1994) had previously measured increased shear strengths in test specimens of up three times the measured quasi-static values when subjected to characteristic vehicle loading. The requirement that enhanced values be used was perceived to be partly due to strain rate enhancement (also observed in similar materials such as concrete by Zielinski and Reinhardt, 1982) and the brittle failure mode found when using the type 9 interface. In the finite element model, when an initially tied node fails the force on adjacent nodes increases dramatically at the next time-step, causing these to then fail in turn. The crack speed is thus dependent on the time-step and node spacing. In reality cracks in such materials do not form in an entirely brittle manner but have a post peak softening response as energy is dissipated. In the model more than one tied node at or near the crack tip could be on a post-peak softening curve at any one time.

Rots and Lourenco (1993) developed a failure criterion that included post peak softening based on fracture energy data from a series of physical tests. More recently Gilbert *et al* (1997), Molyneaux and Gilbert (1997), and Gilbert *et al* (1998) have considered a model, which has similarities to that proposed by Rots. For this model an exponential softening relationship is adopted (Figure 1). This is used to calculate a softening parameter k :

$$k = k^I + k^{II} - 1 \quad (2)$$

This allows a smooth transition between the initial failure surface and the residual failure surface (Figure 1). The initial failure surface comprises the failure criteria of Equ. 1 (above) combined with the Mohr-Coulomb failure criterion in the presence of compressive direct stresses. This approach does however require data to be available on the post peak stress vs. displacement response to enable the mode I and mode II fracture energies to be determined. However, reliable fracture energy data is difficult to obtain and is the subject of current test work by the authors.

Considering Figure 1, if the stresses calculated during the analysis are found to lie outside the initial failure surface they are scaled down using a scale factor f . This factor is then recalculated for each subsequent timestep by taking into consideration the magnitudes of the current plastic tensile and shear deformations (u_t^p , and u_s^p). The areas under the two softening curves used to scale down the stresses are the mode I (tensile) and mode II (shear) fracture energies (G_f^I and G_f^{II} respectively). The ultimate mode I and mode II displacements, u_f^I and u_f^{II} , may be defined as the point on the assumed exponential softening relationship where the interface stress has reached 0.1% of the failure stress.

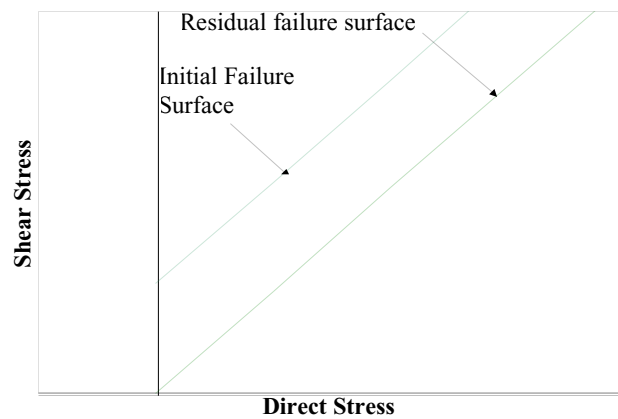


Figure 1 – Failure Surface

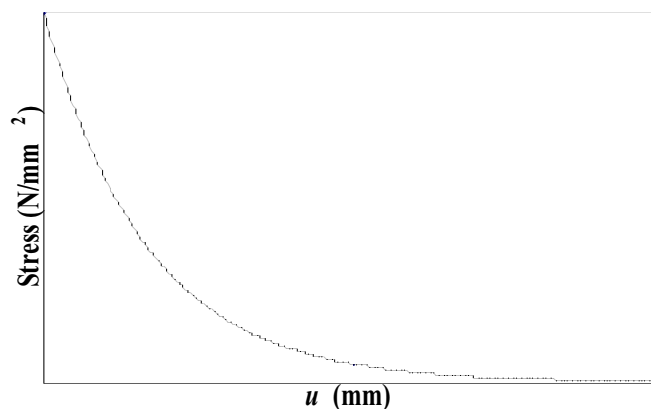


Figure 2 – Exponential Softening Curve

Therefore, given the exponential form of Figure 2:

$$\sigma = \sigma_f e^{(-bu_f)} \quad (3)$$

The fracture energy is thus given as:

$$G_f = \int_{\sigma=0.001\sigma_f}^{\sigma=\sigma_t} \frac{\ln\left(\frac{\sigma}{\sigma_f}\right)}{-b} d\sigma \quad (4)$$

Solving this gives:

$$u^I_f = \frac{-\ln(0.001)G^I_f}{\sigma_f} \quad (5)$$

$$u^{II}_f = \frac{-\ln(0.001)G^{II}_f}{c} \quad (6)$$

Where c is the cohesion (or 'shear bond strength') and k^I and k^{II} referred to in (2) are defined as:

$$k^I = e^{\left\{ \frac{\ln(0.001)u^I_f}{u_f^p} \right\}} \quad (7)$$

$$k^{II} = e^{\left\{ \frac{\ln(0.001)u^{II}_f}{u_f^p} \right\}} \quad (8)$$

The scaling factor f is then defined as:

$$1 \leq f = \sqrt{\left(\frac{\sigma^t_{trial}}{k\sigma^t_f} \right)^2 + \left(\frac{\{\tau_{trial} - \sigma^c_{trial} \tan \phi\}}{kc} \right)^2} \quad (9)$$

Where ϕ is the angle of friction of the masonry joint and where σ^t_{trial} , σ^c_{trial} and τ_{trial} are respectively the trial tensile normal, compressive normal and shear stresses at the joint.

Stresses throughout the softening phase are scaled down as shown in (10), (11) and (12):

$$\sigma^t = \frac{\sigma^t_{trial}}{f} \quad (10)$$

$$\sigma^c = \sigma^c_{trial} \quad (11)$$

$$\tau = \frac{\{\tau_{trial} - \sigma^c_{trial} \tan \phi\}}{f} + \sigma^c_{trial} \tan \phi \quad (12)$$

When $u_p > u_f$ the interface reverts to the standard type 9 model behaviour i.e. contact with friction.

In addition to this softening behaviour, Rots and Lourenco (1993), and Gilbert et al (1998) considered the effects of dilatancy. Dilatancy occurs when there is a separation of the joints perpendicular to the bed joints, which is initiated by a shearing action and caused by the rough surface of the shear failure plane. This action becomes more critical when considering impact events as the inertia of the masonry can lead to high normal stresses. This leads to an increase in the shear resistance of the masonry. The influence of this parameter is the subject of current laboratory test work by the authors.

3.0 Validation of Modelling Strategy

Gilbert *et al* (1998) incorporated the softening formulation described in section 2.0 into LLNL-DYNA. Work on including the formulation in LS-DYNA is expected to commence shortly. The dilatancy effect was also included in this model. Two problems were initially considered; the first was a small-scale triplet sample (see Figure 3) and the second a full-scale laboratory test wall.

The analysis of the triplet showed that the average shear stress at failure was similar over a range of loading rates from 2kN/ms to 40kN/ms when only the softening was incorporated. However, when the dilatancy effect was modelled the higher load rates produced mean shear stresses at failure of up to 3.5 times the values obtained from the lower load rates. For the laboratory walls the model incorporating both softening and dilatancy produced overall displacements that compared well to the experimental data. However, little reliable experimental data to confirm the softening and dilatancy input parameters used for the masonry was available at the time. Therefore, in addition to attempting to incorporate reinforcement into the interface formulations the current work is also evaluating the properties described above by considering:

1. The variation of masonry shear strength under impact loading when compared to quasi-static loading.
2. The variation of masonry tensile strength under impact loading when compared to quasi-static loading.
3. Fracture energy properties (for both mode I and mode II).
4. The effect of dilatancy when masonry fails in shear.

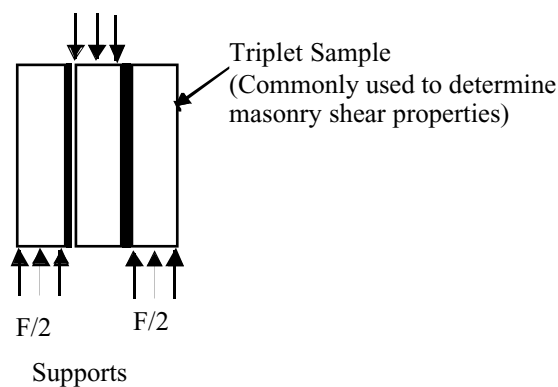


Figure 3 - Triplet Test Arrangement

4.0 Incorporating Reinforcement into the Modelling Strategy

4.1 Test Data

Prior to attempting to model the reinforcement systems a number of full-scale tests have been carried out (URL -1). This is providing useful comparative data for the preliminary modelling work. A series of small scale reinforced masonry tests have also been developed. Parameters such as the pull-out behaviour of the reinforcement will be considered in greater detail than is possible in the larger tests. Once the modelling strategy has been developed modelling will be used to help with the design of future full-scale walls by predicting the behaviour of the walls using various reinforcement options. The future tests will therefore act to validate the modelling.

4.2 The Influence of Bedding Plane Reinforcement

All initial tests on reinforced masonry have used 6mm ribbed stainless steel bars. The initial full-scale test was on a 330mm thick, 19.54m long and 1.09m high brickwork wall constructed using English Garden Wall bond. Reinforcement was positioned on every alternate course on both faces of this wall. An unreinforced wall of identical dimensions was also tested. The two tests confirmed that the behaviour differed extensively between the unreinforced and reinforced walls. It was also shown that there was no improvement in overall behaviour for the reinforced wall when compared to the unreinforced wall.

The reinforced wall produced hinge lines that were 12m apart at the top of the wall. Between these hinge lines the bed joints exhibited extensive splitting and differential out of plane movement of up to 50mm (see Figure 4). These failures in the bedding joints were always on the lower mortar - brick interface and only occurred in bedding joints that contained reinforcement.

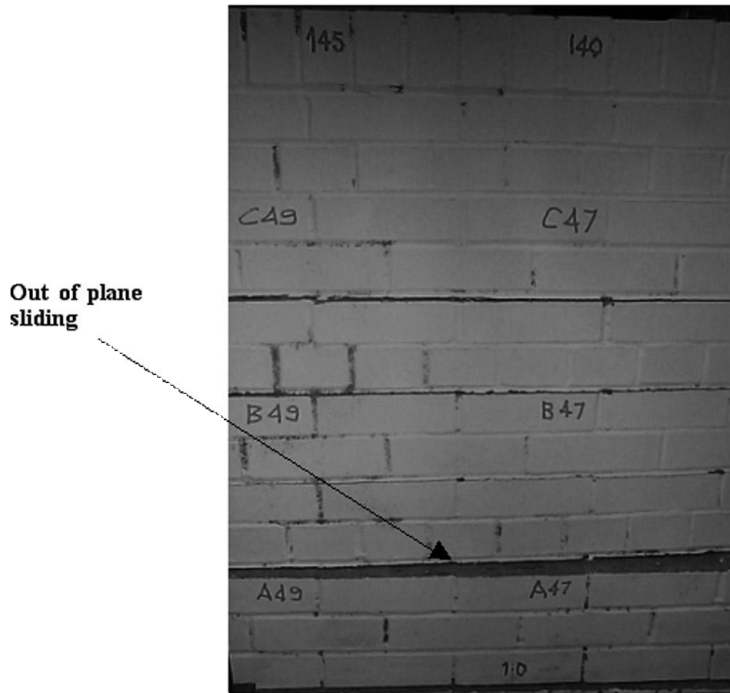


Figure 4 - Lateral Movement between Bed Joints

This splitting and sliding at the bed joint locations may be attributed to a number of factors. Initial tests have shown that during pull-out tests the reinforcement creates a force perpendicular to the bed joint which although is not of significant magnitude to split the bond between the brick and mortar it would in effect reduce the tension limit applying to equation (1). The other factor possibly attributing to this action is that for the masonry to deform it must bend the reinforcement which is firmly anchored at its end. This would therefore create a resultant force acting out of plane to the wall again effectively reducing the shear limit from equation (1).

4.3 Modelling Reinforcement Walls - Initial Strategy

For the reinforced wall models a discrete modelling approach has been employed (e.g. Fig 5). This means that individual masonry units are modelled separately and fracture is only permitted to occur along the mortar joints. This is justified by the fact that the mortar joints form natural planes of weakness. Mortar joints are however not modelled discretely and hence the properties of the discrete units in the model must be representative of the brick-mortar composite. The reinforcement has been modelled using thin shell elements located in the bed-joints between masonry courses. An elasto-plastic material model has been used to model the ribbed stainless steel bar used in the laboratory walls. The centreline of the shell elements has been fixed to coincide with the actual positions of the reinforcement whilst the width of the elements has been taken to be equal to the circumference of these bars. Only one side of the shell elements are fixed to the surfaces of the solid elements making up the masonry units, using the modified type 9 interface formulation described previously (this interface formulation is also used between the surfaces of the solid elements making up all masonry units).

To date the fracture energy associated with debonding of the reinforcement has been taken to be equal to that associated with debonding at a unit-mortar joint. However, it is anticipated that the physical test now underway will show that the debonding of the ribbed reinforcing bar is likely to require considerably higher levels of energy dissipation prior to complete debonding.

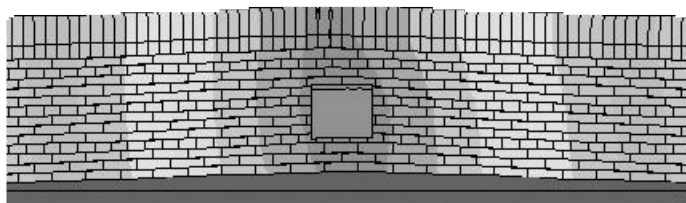


Figure 5 View of a section of a nominally 20m long laboratory wall after impact, showing the interface boundaries, which coincide with the brick joints below the capping course (English Garden Wall bond)

4.4 Preliminary results from reinforced masonry wall models

One of the 9.6m long reinforced brickwork walls tested in the laboratory has been modelled using the strategy described in section 4.3. The maximum out-of-plane displacement and global failure mechanism appeared to be approximated well. Further models constructed to simulate the effects of increasing the amount of reinforcement in the wall have showed that increasing the amount of reinforcement reduces maximum displacement, as expected. However, the splitting action described in 4.2 is not apparent in the model.

One problem encountered in the initial models has been that once the reinforcement in the model becomes debonded, it is then only prevented from penetrating the bedding course on which it was originally connected. This effectively means that it is completely free (Fig 6) whereas, in practice the debonded reinforcement is still contained by the surrounding mortar and masonry.

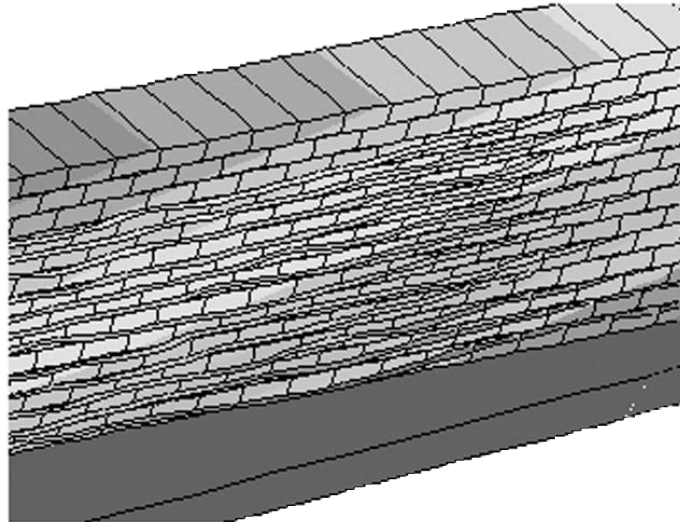


Figure 6 View of section of 9.6m long wall after impact, showing debonded reinforcement (displacements scaled by a factor of 12)

Initially more realistic fracture energy values for the masonry/reinforcement interface will be sought and then included in the models to ascertain whether the above problem persists. If the problem does persist, the type 9 interface could easily be further modified so that, following debonding, the shell elements are permitted to slide freely in the longitudinal direction but are subject to lateral restraint preventing the complete separation that is currently occurring. It seems quite likely that this restraint has an important influence on the performance of the wall, at least when displacements are large.

Numerical models of the 20m long reinforced wall have also been built but results are not yet available.

5.0 Related Work

5.1 Introduction

Current, related work is concerned with the use of LS-DYNA in modelling the behaviour of reinforced and unreinforced masonry arch bridges. The objective of this work is to develop an analysis method capable of predicting the behaviour of unreinforced masonry arch bridges which is flexible enough to allow for the inclusion of, and predict the effects of retrofitted reinforcement. Full scale laboratory tests have been performed on masonry arches for comparison with the numerical work.

Although there are different problems related to the interface modelling than have been identified for the work concerned with the impact behaviour of masonry, the development of a generalised masonry interface algorithm will benefit from this work.

5.2 Modelling Strategy

For all analyses, each brick in the arch barrel was modelled discretely. The type 9 contact interfaces described in section 2.0 were used to simulate the mortar joints. Surface to surface contact interfaces were used to model the interaction between the individual brick rings of the arch barrel to allow delamination. Contact surfaces applied to the interface between the outer ring and the fill material allowed free movement between the elements with only frictional restraint. The fill material was represented with a Drucker Prager soil material (type 193) model.

5.3 Preliminary Results - Unreinforced Arch

Initial analyses were completed on a masonry arch in isolation to test the feasibility of the modelling approach, see Figure 7 below.

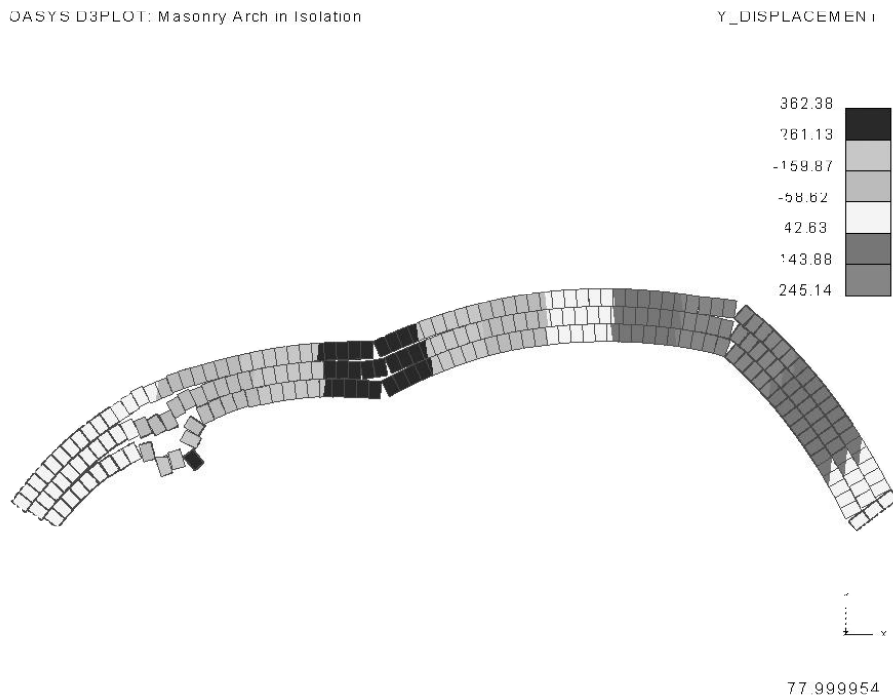


Figure 7: Arch in isolation – Post Collapse Deformations

The mode of failure predicted by the feasibility analyses was encouraging and the model was enhanced to simulate the unreinforced arch test. Fill material was added and a load, linearly increasing with time was applied to the fill above the arch quarter point.

The load above the quarter point was increased until the arch collapsed. Collapse was identified when the reaction at the base fell below the applied load. Figure 8 shows the deformed shape of the model during this analysis.

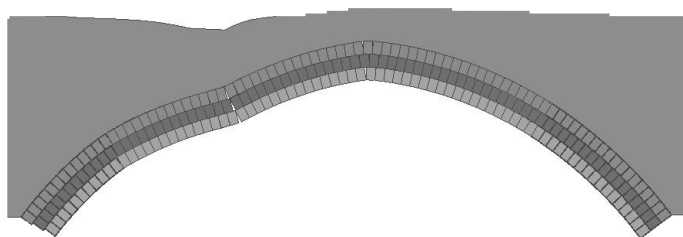


Figure 8: Unreinforced Arch – Deformed Shape

The collapse load predicted by the analysis agreed well with the test results from a full scale unreinforced arch test, and the results were not sensitive to the assumed material parameters.

5.4 Preliminary Results - Reinforced Arch

Reinforcement was incorporated into the model and it was re-analysed. Various configurations of reinforcement were assessed. The results from this work are currently being evaluated.

The reinforcement was modelled using a combination of discrete beam elements to represent single bars and shell elements to model closely spaced parallel bars. Particular care is required when considering reinforcement crossing mortar joints to ensure that the contact surfaces are not locked together. To model the effective reduction in shear stiffness of the reinforcement across the mortar joints a break in the fixity between the bricks and the reinforcement (the width of a typical mortar joint) was included at each joint.

As the analysis simulates retrofitted reinforcement, the model must only include the effects of the reinforcement after the self weight of the structure has been applied. This staged construction simulation was completed by restarting the analysis after the application of self weight. During the application of self weight the reinforcement was included in the model but was assigned with material properties with very low stiffness. The analysis was restarted after the self weight loading had been applied with standard material properties assigned to the reinforcement and the stress initialisation option invoked.

Once the reinforced analysis has been completed and correlated with the test data the sensitivity of the results to assumed input data will be assessed. Any parameters that can be incorporated into the interface algorithm to improve its performance will also be identified.

6.0 Conclusions

1. The type 9 interface in LS-DYNA can be used to connect discrete masonry units when modelling unreinforced masonry. However results may not be objective and the prescribed limiting tensile and shear strengths must be set at high levels in order to obtain reasonable results when modelling vehicle impacts.
2. For the type 9 interface to work satisfactorily using realistic (quasi-static) values for the limiting tensile and shear strengths, it must be modified to incorporate the effects of fracture energy and dilatancy.
3. Initial results from wall models incorporating reinforcement are in reasonable agreement with laboratory test results. However the composite behaviour of the reinforcement and masonry is not fully understood at present. Further tests and modelling work should allow a more appropriate masonry/reinforcement interface formulation to be developed in the future.

6.0 References

6.1 Literature References

BS 6779, pt 4 (1999). *Highway parapets for bridges and other structures – specification for parapets of reinforced and unreinforced masonry construction*, British Standards Institution.

County Surveyors' Society Guidance Note (1995). *The assessment and design of unreinforced masonry vehicle parapets 1-2*. Research Report. Preston: Lancashire County Council.

Gilbert, M., Molyneaux, T.C.K. and Hobbs, B. (1997). Numerical modelling of unreinforced masonry walls subject to lateral impact. *Proc. 11th Int Brick/Block Masonry Conf*, Shanghai. pp473-482.

Gilbert, M., Molyneaux, T.C.K. and Hobbs, B. (1998). A dynamic finite element modelling approach for masonry structures. *Proc. British Masonry Society* **8**.

Molyneaux, T.C.K. (1994). Vehicle Impact on Unreinforced Masonry Parapets. *Proc. Maintenance Engineers Conference*. Publ. Highways Agency, Southwark, London.

Molyneaux, T.C.K., Gilbert, M. and Hobbs, B. (1995). Modelling the response of unreinforced masonry walls to vehicle impacts. *Computer Methods in Structural masonry – 3*. (Eds. J.Middleton and G.N. Pande), Books and Journals International.

pp233-241.

Molyneaux, T.C.K. and Gilbert, M (1997). Modelling masonry joints under impact loading. *Proc. Oasys DYNA3D Users Conf*, London.

Rots, J.G. and Lourenco, P.B. (1993). Fracture simulations of masonry using non-linear interface elements. *Proc. Sixth North American Masonry Conf* (Eds. A.A Hamid and H.G Harris) **2**, pp983-993. Drexel University, Philadelphia, USA.

Zielinski, A.J. and Reinhardt, H.W. (1982). Stress strain behaviour of concrete mortar at high rates of tensile loading. *Cement and Concrete Research* **12**, pp309-319.

6.2 URL References

URL -1 <http://www.liv.ac.uk/~greg99/epsrcgm/genaccess/TestTable1.htm>

Details of full-scale tests to date on the project "Improving the Impact Resistance of Masonry Walls" linked to main page. Visited 05/02/00